

## Aerodynamic control capability of a wing-flap in hypersonic, rarefied regime: Part II

Gennaro Zuppardi\* and Daniele Vangone<sup>a</sup>

*Department of Industrial Engineering, University of Naples "Federico II" Piazzale Tecchio 80,  
80125 Naples, Italy*

*(Received March 15, 2017, Revised May 31, 2017, Accepted July 3, 2017)*

**Abstract.** The attitude control of an aircraft is usually fulfilled by means of thrusters at high altitudes. Therefore, the possibility of using also aerodynamic surfaces would produce the advantage of reducing the amount of fuel for the thrusters to be loaded on board. For this purpose, Zuppardi already considered some aerodynamic problems linked to the use of a wing flap in a previous paper. A NACA 0010 airfoil with a trailing edge flap of 35% of the chord, in the range of angle of attack 0-40 deg and flap deflections up to 30 deg was investigated. Computer tests were carried out in hypersonic, rarefied flow by a direct simulation Monte Carlo code at the altitudes of 65 and 85 km of Earth Atmosphere. The present work continues this subject, considering the same airfoil and free stream conditions but two flap extensions of 45% and 25% of the chord and two flap deflections of 15 and 30 deg. The main purpose is to compare the influence of the flap dimension with that of the flap deflection. The present analysis is carried out in terms of: 1) percentage variation of the global aerodynamic coefficients with respect to the no-flap configuration, 2) increment of pressure and heat flux on the airfoil lower surface due to the Shock Wave-Shock Wave Interaction (SWSWI) with respect to the same quantities with no SWSWI or in no-flap configuration, 3) flap hinge moment. Issues 2) and 3) are important for the design of the mechanical and thermal protection system and of the flap actuator, respectively. Under the above mentioned test and geometrical conditions, the flap deflection is aerodynamically more effective than the flap extension, because it involves higher variation of the aerodynamic coefficients. However, tests verify that a smaller deflection angle involves the advantage of a smaller increment of pressure and heat flux on the airfoil lower surface, due to SWSWI, as well as a smaller hinge moment.

**Keywords:** hypersonic; rarefied aerodynamics; effects of wing-flap extension; shock wave-shock wave interaction; hinge moment; direct simulation Monte Carlo method

---

### 1. Introduction

One of the most pressing problems in an aerospaceplane design, flying through a planet Atmosphere and crossing all rarefaction regimes from free molecular flow to continuum, is the attitude control. This control is usually fulfilled by thrusters at high altitudes and by aerodynamic surfaces (wing-flaps, body-flaps, elevons and so on) at low altitudes. The combination of thrusters

---

\*Corresponding author, Lecturer, E-mail: [zuppardi@unina.it](mailto:zuppardi@unina.it)

<sup>a</sup>M.S. Student, E-mail: [d.vangone@studenti.unina.it](mailto:d.vangone@studenti.unina.it)

and aerodynamic surfaces, also at high altitudes, can provide the indisputable advantage of reducing the amount of fuel for the thrusters to be loaded on the vehicle.

The present paper is the follow-on of an article by the first author (Zuppari 2015), where the effects of a trailing edge flap were computationally evaluated on the flight performances of a wing section. Zuppari carried out the analysis considering a NACA 0010 airfoil with a trailing edge flap of 35% of the chord, in hypersonic, continuum low-density regime at the altitudes of 65 and 85 km of Earth Atmosphere, in the range of angle of attack 0–40 deg and flap deflections up to 30 deg. In the present work, computer tests are performed assuming the same airfoil and test conditions, but two different flap extensions of 45% and 25% of the chord and a flap deflection of 15 deg.

Because of the difficulty of reproducing experimentally the test conditions, or Mach, Reynolds and Knudsen numbers of an aerospaceplane, in the previous as well as in the present paper, the study has been carried out computationally; more specifically, a Direct Simulation Monte Carlo (DSMC) code has been used. As well known, the DSMC method (Bird 1998, 2013), (Shen 2005) provides the solution of a flow field in rarefied regime. DSMC overcomes the failure of the Navier-Stokes equations due to the failure of the phenomenological equations of Newton, Fourier and Fick in rarefied flow. In addition, the use of a DSMC code is mandatory for this kind of application. In fact, the complexity of the flow field on the lower surface of the airfoil with deflected flap could make difficult the solution of the flow field by “classic” Computational Fluid Dynamics (CFD) codes. This complexity is due to the shock wave/boundary layer interaction linked to the compression ramp produced by the flap deflection and to the interaction of this shock wave with the one coming from the airfoil leading edge. Since 90’s of the 20<sup>th</sup> century, the DSMC method has been widely accepted for the solution of flow fields of satellites, capsules, space and Aero-assisted Flight Experiments (AFE) vehicles (see references in Shen 2005).

It is well known that when the solution of a problem relies on a computational approach, it is always necessary to verify the reliability of the calculations. Unfortunately, due to the very special test conditions associated with high numbers of Mach and Knudsen, the lack of comparison data for the NACA 0010 airfoil does not make possible a direct validation of the results. Nevertheless, the validity of results is supported both by the reliability of the used computer code (DS2V 4.5 64 bits, Bird 2012) that is widely accepted by the worldwide scientific community and by the physical correspondence with what predicted by the theory of the aerodynamic phenomenon.

As already pointed out by Zuppari (2015), the investigated problem is essentially of academic interest. In fact, equilibration of both forces and moments around the center of gravity and the attitude control of a whole vehicle are much more complex. The spirit of the two papers is to provide gross information for the design of aerodynamic control surfaces. This has to be a compromise solution of aerodynamic capability in changing aerodynamic coefficients and therefore in controlling a spacecraft attitude and the intensity of unwanted phenomena such as Shock Wave-Boundary Layer Interaction (SWBLI) and Shock Wave-Shock Wave Interaction (SWSWI). Physics and basic phenomena of SWBLI and SWSWI were widely described by Anderson (1989) and Bertin (1994) respectively, and summarized by Zuppari (2015). The compromise solution is among the geometric parameters of the control surfaces: length and deflection angle. The results of the computations of forces and moments of an insulated airfoil, carried out in the previous and in the present papers, are only indicative. Furthermore, the hypersonic flight of an aerospaceplane could be strongly affected by the shock wave interactions because of the impact on the spacecraft stability, aerodynamic or pressure loads and heat flux. These phenomena lead to the development of technological solutions necessary to assure a continuous attitude control of a spacecraft and to the design of a mechanical and thermal

protection system.

Also in the present paper, the analysis relies on the evaluation of the flap capability in changing aerodynamic force and longitudinal moment coefficients. The unwanted phenomenon of pressure and heat flux increments, produced by the flap deflection along the airfoil lower surface, is considered. The related increment of the hinge moment is included in the analysis. The last two issues are important for the design of the mechanical and thermal protection system and of the flap actuator, respectively.

## 2. Direct simulation Monte Carlo method and DS2V-64bits code

The Direct Simulation Monte Carlo (DSMC) method is a computational, statistical and stochastic method providing simulated flows from free molecular to continuum low-density regimes. DSMC relies on the kinetic theory of gases and considers the gas as made of millions of simulated molecules, each one representing a large number of real molecules (in the present computations of the order of  $10^{14}$ ) in the physical space. The evolution of the molecules, in terms of velocity, spatial coordinates and internal thermodynamic status, is produced by intermolecular and molecule-surface collisions within the simulated physical space. This is divided into cells both for selecting the colliding molecules (collision cells) and for sampling the thermo-fluid-dynamic parameters (sampling cells). The molecules in a cell represent those at the same location in the physical field. The method does not suffer from numerical instabilities but it is inherently unsteady with a steady solution achievable after a sufficiently long simulation time.

The DSMC code used in the previous and in the current study is the general 2D/axisymmetric code DS2V-64bits (Bird 2012). It implements the Gupta-Yos-Thompson (Gupta *et al.* 1989) chemical model for air, which is considered made of five neutral reacting species ( $O_2$ ,  $N_2$ ,  $O$ ,  $N$  and  $NO$ ). The model consists of 23 forward/reverse chemical reactions. DS2V is a “sophisticated” code. A DSMC code is labelled “sophisticated” if it implements computing procedures achieving both greater efficiency and accuracy with respect to a “basic” DSMC code. More specifically, it: (1) divides the computational volume into two sets of cells (collision and sampling) with the related cell adaptation (Bird 2006, Bird *et al.* 2009, Gallis *et al.* 2009), (2) implements a procedure for the selection of the colliding molecules from the “nearest collision” pair within the cell, (3) generates automatically computational parameters according to the input number of megabytes and free stream molecule density, (4) provides an optimal time step, (5) avoids sequential collision between the same collision pair, (6) allows the user to evaluate the quality of the computation.

The ratio between the molecule mean collision separation ( $mcs$ ) and the mean free path ( $\lambda$ ) in each collision cell is the parameter allowing the evaluation of the quality of a DSMC run;  $mcs/\lambda$  has to be less than unity everywhere in the computational domain for a good quality of a run. Bird (2006) suggests that the  $mcs/\lambda$  ratio should be less than 0.2 for an optimal quality of the run. This is the most important parameter because it provides a measure of the adequacy of both the numbers of simulated molecules and of the collision cells.

Finally, the stabilization of a DS2V calculation is achieved when the profile of the simulated molecules as a function of the simulated time becomes jagged and is included within a band, which defines the standard deviation of the number of simulated molecules.

## 3. Test conditions and quality of the runs



Fig. 1 NACA 0010 airfoil in clean configuration (a) and with hinge positions  $x/c=0.55$  (b),  $x/c=0.65$  (c) and  $x/c=0.75$  (d):  $\delta=15$  deg

Table 1 Input data to DS2V-64bits and free stream aerodynamic parameters

h (km)	$T_\infty$ (K)	$\rho_\infty$ (kg/m <sup>3</sup> )	$N_\infty$ (m <sup>-3</sup> )	$V_\infty$ (m/s)	$M_\infty$	$Re_{\infty c}$	$Kn_{\infty c}$
85	189	$8.22 \times 10^{-6}$	$1.71 \times 10^{20}$	7355	26.7	$9.50 \times 10^3$	$4.0 \times 10^{-3}$
65	233	$1.63 \times 10^{-4}$	$3.39 \times 10^{21}$	5163	16.8	$1.11 \times 10^5$	$2.1 \times 10^{-4}$

Table 2 Sensitivity analysis of the wall temperature and chemical status:  $h=65$  km,  $x_h/c=0.65$

	$C_l$	$C_d$	$C_l/C_d$	$C_F$	$C_{mz}$
$T_w=300$ K, NC	0.3464	0.2355	1.4707	0.4189	-0.2029
$T_w=1052$ K, NC	0.3435	0.2401	1.4306	0.4191	-0.2036
$T_w=300$ K, FC	0.3411	0.2386	1.4293	0.4162	-0.2017

The DSMC computations are carried out on the “classic” NACA 0010 airfoil in clean or no-flap and flapped configurations. Figs. 1(a)-(d) show the airfoil geometries in clean configuration 1(a), with flap extension of 45% 1(b), 35% 1(c) and 25% 1(d) of the chord (c); the hinge is located along the chord at  $x/c=0.55$ , 0.65 and 0.75, respectively. Since the chord is 2 m, the flap hinge is set at  $x=1.10$ , 1.30 and 1.50 m, respectively. In the three pictures, the flap deflection angle ( $\delta$ ) is 15 deg.

The airfoil surface is approximated by 1000 flat panels (500 on the lower surface and 500 on the upper surface). The 2-D computing domain is a rectangle:  $L_x=2.5$  m,  $L_y=1.1$  m.

Table 1 reports input data to DS2V and some free stream aerodynamic parameters. Velocity ( $V_\infty$ ) is evaluated at the altitudes (h) of 65 and 85 km along a typical re-entry trajectory of the FTB-X vehicle (Zuppardi *et al.* 2011). Temperature ( $T_\infty$ ), density ( $\rho_\infty$ ) and number density ( $N_\infty$ ) are provided by the U.S. Standard Atmosphere 1976. Air composition is standard or, in terms of molar fractions ( $\alpha$ ),  $\alpha_{N_2}=0.79$  for Nitrogen and  $\alpha_{O_2}=0.21$  for Oxygen. The Reynolds ( $Re_{\infty c}$ ) and the Knudsen ( $Kn_{\infty c}$ ) numbers are based on the airfoil chord. The Knudsen number verifies that the flow field is practically in continuum low-density regime at these altitudes. In fact, according to Moss (1995), the transitional regime is defined by:  $10^3 < Kn_{\infty c} < 50$ .

The runs are carried out at the angles of attack ( $\alpha$ ) ranging from 0 to 40 deg with an interval of 5 deg. The analysis of the results relies on 72 runs: 36 runs were already performed by Zuppardi (2015) on the airfoil in clean and flapped configurations with hinge position at  $x/c=0.65$  and flap deflection of 30 deg.

The indetermination of the airfoil surface temperature is taken into account by means of a preliminary sensitivity analysis. The calculation of the aerodynamic force coefficients ( $C_l$ ,  $C_d$ ,  $C_F$  and  $C_{mz}$ ) is done at: i) low temperature of  $T_w=300$  K and Non-Catalytic surface (NC), ii) adiabatic wall temperature ( $T_w=T_{aw}$ ) and non-catalytic surface, iii)  $T_w=300$  K and Fully-Catalytic surface (FC). The implemented chemical surface reactions are:  $O+O \rightarrow O_2$  and  $N+N \rightarrow N_2$ . The fully-catalytic condition is fixed in DS2V by setting the probability of each surface reaction to one.

The computations are carried out at the intermediate conditions of:  $x_h/c=0.65$ ,  $\alpha=20$  deg and  $\delta=15$  deg. In the present tests the adiabatic wall temperature, computed by DS2V, is  $T_{aw}=1052$  K. As reported in Table 2, the influence on the aerodynamic coefficients is practically negligible.

Table 3 DS2V run parameters

h (km)	$N_m$	$N_c$	$N_s$	mcs/ $\lambda$	$t_s/t_f$
65	$4.5 \times 10^7$	$3.2 \times 10^6$	$9.7 \times 10^4$	0.50	2.7
85	$4.8 \times 10^7$	$2.9 \times 10^6$	$1.1 \times 10^4$	0.10	3.9

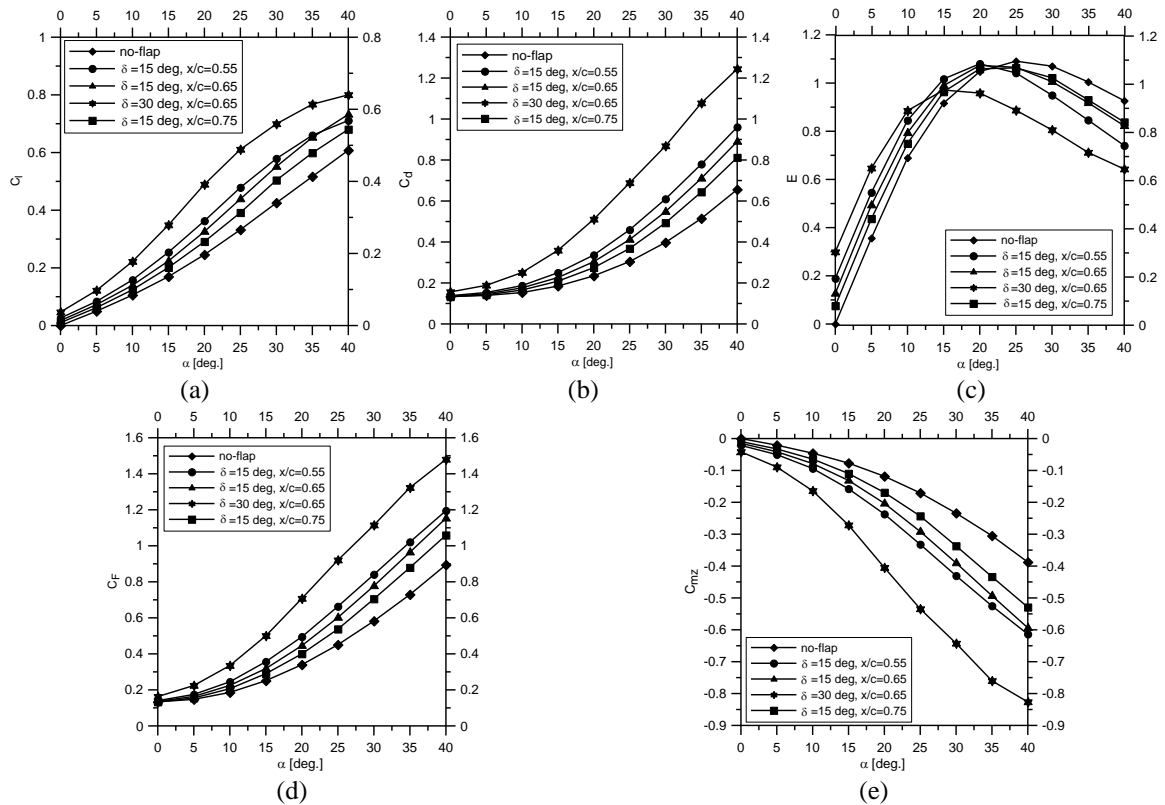


Fig. 2 Profiles of lift (a) and drag (b) coefficients, aerodynamic efficiency (c), aerodynamic force (d) and longitudinal moment (e) coefficients as functions of the angle of attach:  $h=85$  km

Certainly, both the wall temperature and the wall chemical behavior (catalytic/non-catalytic) of a surface play an important role in thermal problems, as per computation of heat flux. However, as the subject of the present paper is related practically only to the force and moment coefficients, the choice of the wall temperature and its chemical behavior is marginal. All computations are carried out with  $T_w=300$  K and non-catalytic surface, assuming a constant temperature distribution along the airfoil surface.

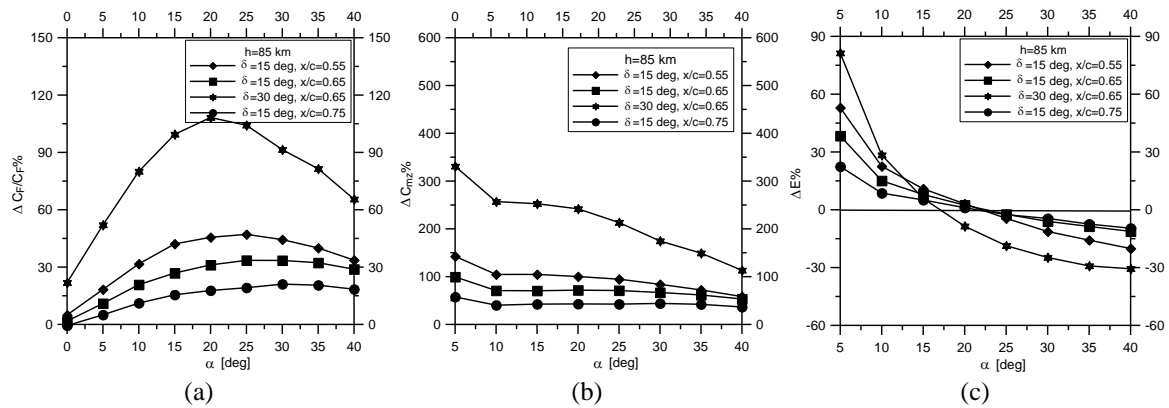
The present (36) runs satisfy also the requirements of good quality, in terms of both DSMC and fluid-dynamic criteria. For example, Table 3 reports some parameters of two illustrative runs at each altitude such as: numbers of simulated molecules ( $N_m$ ), collision cells ( $N_c$ ), sampling cells ( $N_s$ ), ratio  $mcs/\lambda$  and ratio of the simulation time ( $t_s$ ) to the time ( $t_f$ ) required to travel a distance equal to the airfoil chord at the free stream velocity. These parameters are practically met in each run. Even though the value of  $mcs/\lambda$  at  $h=65$  km does not reach the optimal limit value of 0.2, it is smaller than unity. Furthermore, the ratio  $t_s/t_f$ , reasonably satisfies the criterion for the stabilization of the run from a fluid-dynamic point of view ( $t_s/t_f=O(10)$ ).

Table 4 Maximum percentage variation of the force coefficient ( $C_F$ )

h (km)	$x/c=0.55, \delta=15^\circ$	$x/c=0.65, \delta=15^\circ$	$x/c=0.75, \delta=15^\circ$	$x/c=0.65, \delta=30^\circ$
65	47	34	21	108
85	58	41	27	149

Table 5 Maximum percentage variation of the force coefficient ( $C_{mz}$ )

h (km)	$x/c=0.55, \delta=15^\circ$	$x/c=0.65, \delta=15^\circ$	$x/c=0.75, \delta=15^\circ$	$x/c=0.65, \delta=30^\circ$
65	143	100	57	331
85	194	138	80	531

Fig. 3 Percentage variations of the force (a) and moment (b) coefficients and aerodynamic efficiency (c) as function of the angle of attack:  $h=85$  km

## 4. Analysis of the results

### 4.1 Force and moment coefficients

Figs. 2(a)-(e) show the profiles of the lift ( $C_l$  (a)) and the drag ( $C_d$  (b)) coefficients, aerodynamic efficiency ( $E=C_l/C_d$  (c)), aerodynamic force coefficient ( $C_F$ ,  $C_F = \sqrt{C_l^2 + C_d^2}$  (d)), longitudinal moment coefficient ( $C_{mz}$  (e); the pole is the airfoil leading edge), as functions of the angle of attack for the three hinge positions at the altitude of 85 km. Each plot shows also the results of the airfoil in no-flap configuration and those with  $\delta=30$  deg and  $x/c=0.65$ , already computed by Zuppardi (2015). The maximum aerodynamic efficiency is not strongly dependent on the flap extension for  $\delta=15$  deg; its values are 1.49, 1.51, 1.39 at  $h=65$  km and 1.08, 1.07, 1.06 at 85 km for the three hinge positions, respectively, and are met at an angle of attack of about 20 deg. On the contrary, the flap deflection of 30 deg involves a more substantial variation of the maximum efficiency; its value is 1.26 at  $\alpha=10$  deg and 0.97 at  $\alpha=15$  deg for  $h=65$  and 85 km, respectively.

A quantitative assessment of the flap capability to keep/change the attitude can be performed by the percentage variations of the force and of the leading edge moment coefficients with respect to those in no-flap configuration. Figs. 3(a)-(b) and 4(a)-(b) show the profiles of the percentage variations of  $C_F$  and  $C_{mz}$  as functions of the angle of attack at the two altitudes. The maximum effect of the flap deflection is met

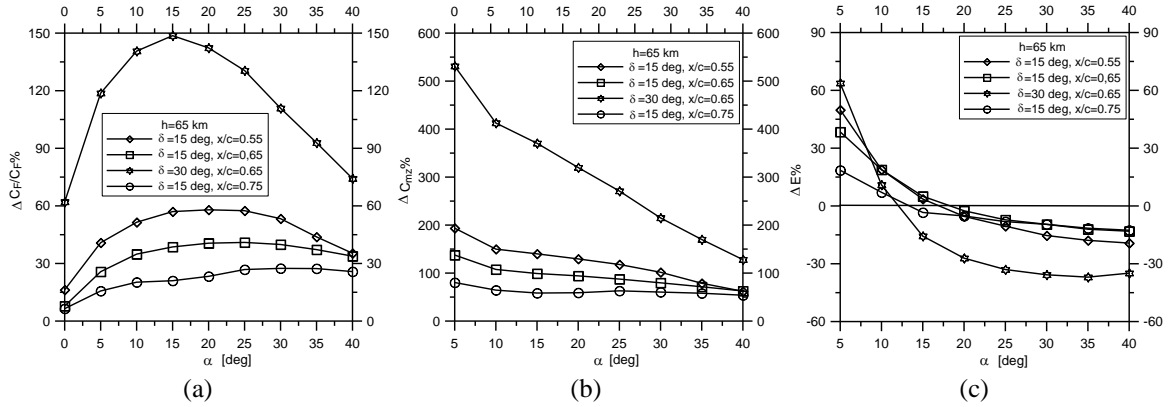


Fig. 4 Percentage variations of the force (a), moment (b) coefficients and aerodynamic efficiency (c) as function of the angle of attack:  $h=65$  km

around the maximum aerodynamic efficiency angle for the aerodynamic force and at  $\alpha=5$  deg for the longitudinal moment. The effects of the flap deflection is far stronger than those of the flap extension. Tables 4 and 5 report the maximum percentage variations of  $C_F$  and  $C_{mz}$ . For the sake of completeness, Fig. 3(c) and Fig. 4(c) show the profiles of the percentage variation of the aerodynamic efficiency. The flap deflection produces an effect stronger than that one of the flap extension even in terms of variation of this parameter.

#### 4.2 Pressure and heat flux

As said before, the SWSWI involves the shock wave coming from the airfoil leading edge and that one coming from the hinge produced by the concave wedge formed by the flapped airfoil lower surface. As the interacting waves are of the same family, the intensity of the “new” shock wave is higher than that one coming from the hinge and comparable with that one on the airfoil leading edge (Zuppardi 2015). Therefore, pressure and heat flux on the airfoil lower surface are even one order of magnitude higher than the same quantities computed in clean configuration.

In order to show the influence of the flap deflection angle on the flow field, Figs. 5(a)-(b) show the 2-D maps of pressure and Figs. 5(c)-(d) show the 2-D maps of temperature at the most severe test conditions of  $h=65$  km and  $\alpha=40$  deg. These test conditions are of interest for an aerospaceplane. In fact, the angle of attack of 40 deg was typical for the Space Shuttle during the re-entry. Furthermore, Zuppardi computed the maximum heat flux on the nose of SpaceLiner (Zuppardi *et al.* 2014) at the altitude of 65 km. The flap deflections are:  $\delta=15$  deg for Fig. 5(a) and Fig. 5(c),  $\delta=30$  deg for Fig. 5(b) and Fig. 5(d). For completeness, the streamlines are also drawn on the pressure maps. The pictures indicate that a flap deflection of 15 deg is not enough to generate meaningful SWSWI effects. On the opposite, these effects are much stronger for  $\delta=30$  deg. This remark is supported also by Figs. 6(a)-(b) where a zoom of the streamline patterns at the hinge position is reported for the two deflection angles. The streamline patterns identify the separation bubble and clearly show that its extension is larger for  $\delta=30$  deg.

In Figs. 5(a) to 5(d) the flow expansion on the airfoil upper surface near the location of the camber deflection does not appear. This is due to the synergic effects of the free stream flow rarefaction and of the high angle of attack; the upper surface of the airfoil at  $\alpha=40$  deg is

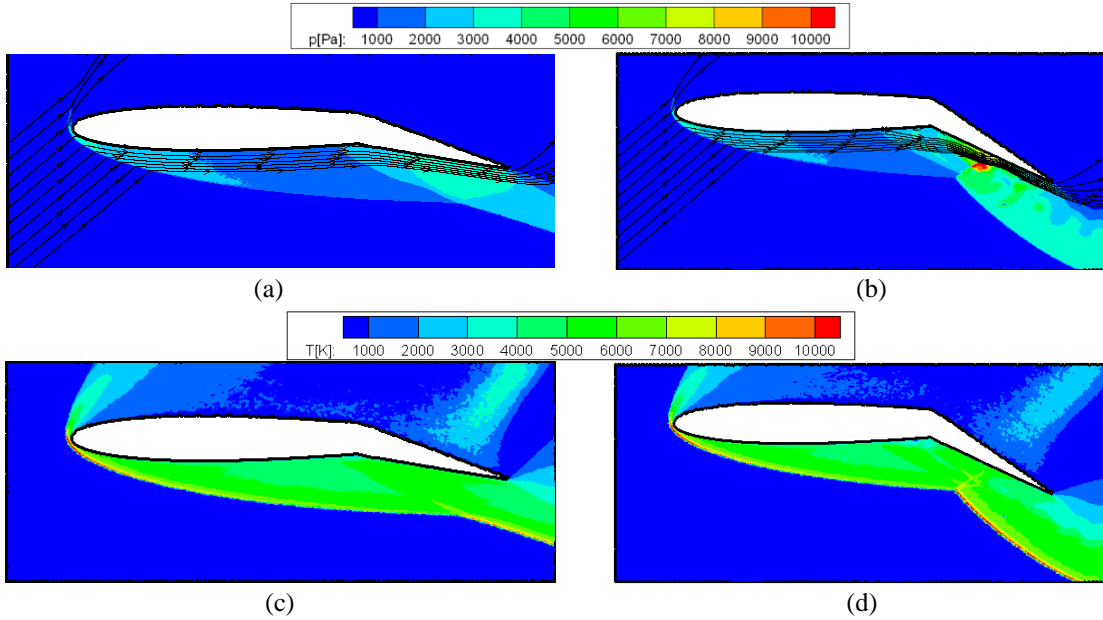


Fig. 5 2-D pressure and temperature maps for  $\delta=15$  deg (a), (c) and  $\delta=30$  deg (b), (d):  $h=65$  km,  $\alpha=40$  deg  $x/c=0.65$

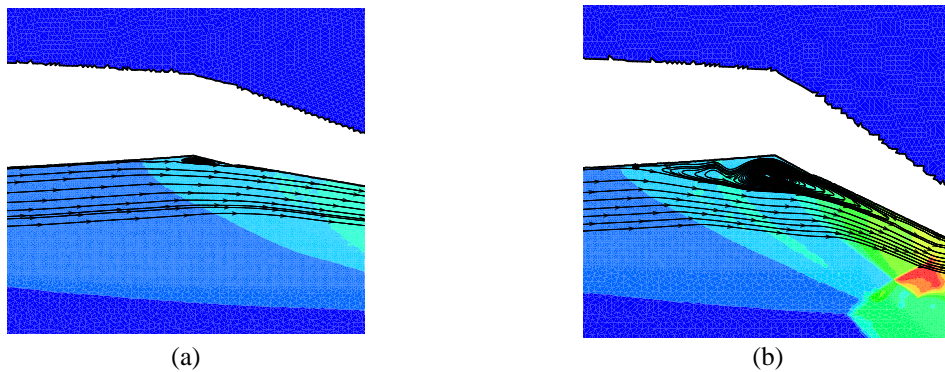


Fig. 6 Zoom of the 2-D pressure maps and related streamline at the hinge position with  $\delta=15$  deg (a) and  $\delta=30$  deg (b):  $h=65$  km,  $\alpha=40$  deg

practically in aerodynamic shadow. The peak of pressure in the flow field, the red spot shown in Fig. 5(b) and also in Fig. 6(b), at about the middle of the flap, is due to SWSWI. This, in turn, produces a pressure and heat flux peaks on the surface of the flap, as shown in Fig. 7(a) and in Fig. 8(a).

Figs. 7(a)-(b) show the profiles of pressure and heat flux along the airfoil lower surface as functions of the curvilinear abscissa ( $s$ ), at  $h=65$  km,  $\alpha=40$  deg and  $\delta=15$  deg for the three flap extensions. Due to the shock wave stemming from the hinge, both pressure and heat flux increase. Since the flap deflection is the same for the three flap extensions and the SWSWI effect is negligible, both quantities are practically constant along the flap surface. Both sets of profiles are barely able to show the small separation bubble at the hinge position. This separation bubble is

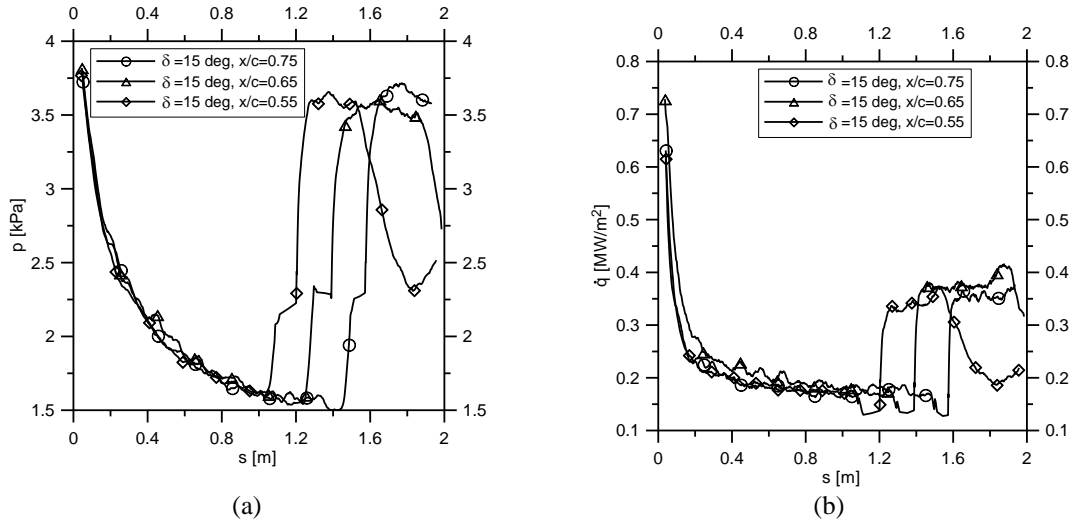


Fig. 7 Profiles of pressure (a) and heat flux (b) along the airfoil lower surface:  $h=65$  km,  $\alpha=40$  deg,  $\delta=15$  deg

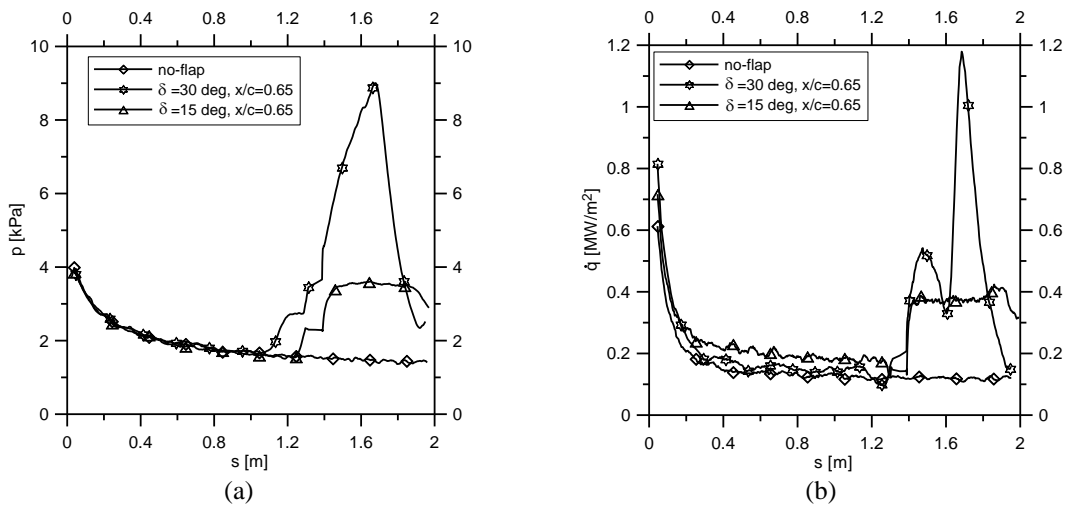


Fig. 8 Profiles of pressure (a) and heat flux (b) along the airfoil lower surface:  $h=65$  km,  $\alpha=40$  deg,  $x/c=0.65$

visualized by means of a very small plateau on the heat flux profile. On the contrary, the abrupt decrease of heat flux, shown in Fig. 8(b), clearly identifies the separation bubble for  $\delta=30$  deg. Furthermore, Figs. 8(a)-(b) indicate that the above mentioned increments of pressure and heat flux, produced by the higher flap deflection, are much more consistent. The heat flux profile shows two relative maxima: the first one is due to the shock wave stemming from the hinge and the second one is due to SWSWI. The latter is about 2.5 times higher than the former. The percentage variations of the maximum values of pressure and heat flux, with respect to the same quantities in no-flap conditions, are reported in Table 6 at the two altitudes and for the two flap deflections. The increments of heat flux and pressure computed with  $\delta=30$  deg are at least three times larger than those computed with  $\delta=15$  deg.

Table 6 Percentage increments of heat flux and pressure:  $\alpha=40$  deg,  $x/c=0.65$ 

h (km)	$\Delta q\%, \delta = 15^\circ$	$\Delta p\%, \delta = 15^\circ$	$\Delta q\%, \delta = 30^\circ$	$\Delta p\%, \delta = 30^\circ$
65	67	150	1150	571
85	82	97	286	341

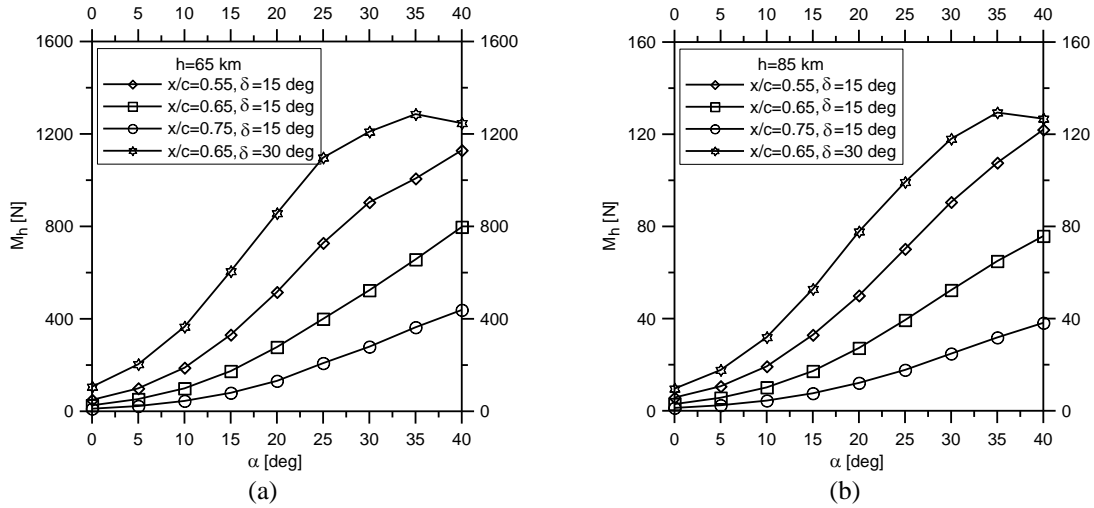
Fig. 9 Profiles of hinge moment at  $h=65$  (a) and  $h=85$  (b) km as functions of the angle of attack

Table 7 Maximum hinge moment per unit length (N)

h (km)	$x/c=0.55, \delta=15$ (deg)	$x/c=0.65, \delta=15$ (deg)	$x/c=0.75, \delta=15$ (deg)	$x/c=0.65, \delta=30$ (deg)
85	122	76	38	129
65	1129	798	438	1286

### 4.3 Hinge moment

The hinge moment ( $M_h$ ) is computed by integrating the contributions of the components of the aerodynamic forces  $F_{x_i}$  and  $F_{y_i}$  (the  $x$  axis is along the airfoil chord) on each aerodynamic panel of the flap surface

$$M_h = \sum_{i=1}^{N_p} (F_{y_i}(x_i - x_h) - F_{x_i}(y_i - y_h)) \quad (1)$$

where  $N_p$  is the number of panels,  $x_i$  and  $y_i$  are the coordinates of the panel center where  $F_{y_i}$  and  $F_{x_i}$  are applied and  $x_h$  and  $y_h$  are the hinge coordinates.  $F_{y_i}$  and  $F_{x_i}$  read

$$F_{y_i} = (p_i \cos \vartheta_i - \tau_i \sin \vartheta_i) \Delta s_i \quad (2a)$$

$$F_{x_i} = (p_i \sin \vartheta_i + \tau_i \cos \vartheta_i) \Delta s_i \quad (2b)$$

where  $p_i$  and  $\tau_i$  are the pressure and the shear stress on a panel,  $\vartheta_i$  is the panel angle with respect to the chord and  $\Delta s_i$  is the panel surface.

Figs. 9(a)-(b) show the hinge moment profiles as function of the angle of attack for the three flap extensions and the two flap deflections. The profiles are qualitatively the same at the two altitudes and the differences, practically of an order of magnitude, are due to the free stream density (see Table 1). The maximum values of the hinge moments (Table 7) provide information both for the design of the flap actuator and the power to be supplied. Once again, a flap deflection of  $\delta=30$  deg involves the highest hinge moment. For example, the percentage variations of the hinge moment at  $h=65$  km are about 14%, 61% and 194% higher than those of the flap at  $x/c=0.55, 0.65, 0.75$  with  $\delta=15$  deg.

## 5. Conclusions

The present work has been the follow-on of a previous article by the first author where the feasibility of an aerodynamic control by means of a trailing edge flap was analyzed.

In this paper, the effects of the flap deflection angle and of the flap extension have been compared. The study has been carried out computationally by a direct simulation Monte Carlo code (DS2V-64 bits). The computations have been performed in hypersonic, continuum low-density regime on a NACA 0010 airfoil (2 m chord) with no-flap and three flap extensions of 45%, 35% and 25% of the chord, at the altitudes of 65 and 85 km, in the interval of angles of attack 0-40 deg and with flap deflections of 15 and 30 deg.

The flap effects have been quantified in terms of the percentage variation of the global aerodynamic coefficients, increments of pressure and heat flux on the airfoil lower surface due to shock wave-shock wave interaction and hinge moment.

Even though the flap deflection is aerodynamically more effective than the flap extension in keeping/changing attitude, the current computations have verified that a more extended flap, with a smaller deflection angle, satisfies a good compromise among the capability of changing aerodynamic force and moment, the increment of mechanical (pressure) and thermal (heat flux) loads on the airfoil lower surface and the increment of hinge moment.

A smaller flap deflection angle involves smaller increments of mechanical and thermal loads on the airfoil lower surface, therefore lighter and cheaper protection systems as well as a less powerful flap actuator.

## References

- Anderson, J.D. (1989), *Hypersonic and High Temperature Gas Dynamics*, McGraw-Hill International Editions, New York, U.S.A.
- Bertin, J.J. (1994), *Hypersonic Aerothermodynamics*, AIAA Education Series, Washington, U.S.A.
- Bird, G.A. (1998), *Molecular Gas Dynamics and Direct Simulation Monte Carlo*, Clarendon Press, Oxford, U.K.
- Bird, G.A. (2006), "Sophisticated versus simple DSMC", *Proceedings of the 25th International Symposium on Rarefied Gas Dynamics*, Saint Petersburg, Russia, July.
- Bird, G.A., Gallis, M.A., Torczynski, J.R. and Rader, D.J. (2009), "Accuracy and efficiency of the sophisticated direct simulation monte carlo algorithm for simulating non-continuum gas flows", *Phys. Flu.*, **21**(1), 017103.
- Bird, G.A. (2012), *Visual DSMC Program for Two-Dimensional Flows*, the DS2V Program User's Guide

- Version 4.5, Sidney, Australia.
- Bird, G.A. (2013), *The DSMC Method, Version 1.1* (Amazon, ISBN 9781492112907), Charleston, U.S.A.
- Gallis, M.A., Torczynski, J.R., Rader, D.J. and Bird, G.A. (2009), "Convergence behavior of a new DSMC algorithm", *J. Comput. Phys.*, **228**(12), 4532-4548.
- Gupta, R.N., Yos, J.M. and Thompson, R.A. (1989), *A Review of Reaction Rates and Thermodynamic Transport Properties for an 11-Species Air Model for Chemical and Thermal Non-Equilibrium Calculations to 30,000 K*, NASA TM 101528.
- Moss, J.N. (1995), *Rarefied Flows of Planetary Entry Capsules*, Special course on "Capsule Aerothermodynamics", Rhode-Saint-Genèse, Belgium, May, AGARD-R-808, 95-129.
- Shen, C. (2005), *Rarefied Gas Dynamic: Fundamentals, Simulations and Micro Flows*, Springer-Verlag, Berlin, Germany.
- Zuppari, G., Visone, G., Votta, R. and Schettino, A. (2011), "Analysis of aerodynamic performances of experimental flying test bed in high-altitude flight", *J. Aerosp. Eng.*, **225**(3), 247-258.
- Zuppari, G., Morsa, L., Sippel, M. and Schwanekamp, T. (2014), "Aero-thermo-dynamic analysis of the SpaceLiner-7.1 vehicle in high altitude flight", *Proceedings of the 29<sup>th</sup> International Symposium on Rarefied Gas Dynamics*, Xian, China, July.
- Zuppari, G. (2015), "Aerodynamic control capability of a wing-flap in hypersonic, rarefied regime", *Adv. Aircraft Spacecraft Sci.*, **2**(1), 45-56.